 cmes, vol.5, no.5, pp.423-434, 2004

Hierarchical Vector Finite Elements with p-Type non-Overlapping Schwarz Method for Modeling Waveguide Discontinuities

Jin Fa Lee[1], Robert Lee[2], and Fernando Teixeira[3]

Abstract: This paper presents the application of a p-type Multiplicative Schwarz Method (pMUS) for solving three dimensional waveguide discontinuity with arbitrary shapes. The major ingredients of current approach are: a hierarchical curl-conforming basis functions that incorporates an in-exact Helmholtz decomposition; and, treating each polynomial space (or basis functions group) as an abstract grid/domain in the Schwarz method. Various numerical examples are studied using the proposed approach. The performance has been compared to currently available commercial software and demonstrated superior performance in terms of accuracy as well as efficiency.

1 Introduction

Waveguide discontinuities are still major components in RF/microwave circuits/systems, subsequently, predictions of their performances and characteristics are still having major impact on microwave engineering. Applications include waveguide couplers, waveguide filters, waveguide duplexers, and waveguide converters etc. Except for a few canonical problems, most of the waveguide discontinuity analyses require numerical methods. Popular methods that helped greatly in CAD/CAE for microwave engineering are: method of moments [Bornemann, Rosenberg, Amari, and Vahldieck (1999)][Amari, Bornemann, Laisne, and Vahldieck (1996)], mode matching [Papziner and Amdt (1993)], finite difference methods (FDMs) [Li, Zhang, and Nakhla (1996)] and finite element methods (FEMs) [Lee (1990)]. Also, keep in mind that these methods are not necessarily against/competing with each other, in fact, often than not, they are used together by engineers to analyze real-life waveguide components.

This paper specifically addresses the issues of employing vector finite elements method [Lee (1990)][Nedelec (1980)][Lee, Sun, and Cendes (1991)] to simulate three-dimensional waveguide components. It is well known that the benefits of using FEMs are flexibility of modeling arbitrary problem geometries and capability to include various material properties (inhomogeneities) of the devices. However, it is also well known that PDE methods, such as FEMs, are inefficient for solving large problems where matrices with hundreds of thousands of unknowns need to be solved. The aim of this contribution is to introduce several recent developments in FEM technologies, and to demonstrate the combination of these techniques results in order-of-magnitude speed-up compared to currently available FEM approaches to solve Maxwell equations. In particular, two new developments are discussed in full here: hierarchical vector basis that is constructed according to a discrete in-exact Helmholtz decomposition, and a p-type multiplicative Schwarz method (pMUS) for solving the matrix equations.

Presently, it is commonly accepted that the use of the curl-conforming vector finite element basis functions, tangential vector finite element methods (TVFEMs) [Lee, Sun, and Cendes (1991)] inspired by Nedelec [Nedelec (1980)], is a reliable way to solve Maxwell equations in the frequency domain. Most efforts recently turn to build higher order basis functions. Among them, we believe the hierarchical constructions of the basis functions proposed in Ref. [Webb][Sun, Lee, and Cendes (2001)] are most appropriate for efficient FEM implementations. Hierarchical basis functions enable many highly efficient matrix solution processes, such as multigrid (MG) methods [Hiptmair (1998)] and

[1] ElectroScience Lab., Electrical Engineering Dept., The Ohio State University, Columbus, OH 43212 USA (telephone: 614-292-7270, e-mail: jinlee@ee.eng.ohio-state.edu).

[2] ElectroScience Lab., Electrical Engineering Dept., The Ohio State University, Columbus, OH 43212 USA (e-mail: lee@ee.eng.ohio-state.edu).

[3] ElectroScience Lab., Electrical Engineering Dept., The Ohio State University, Columbus, OH 43212 USA (e-mail: teixeira@ee.eng.ohio-state.edu).

domain-decomposition (DD) methods [Smith, Bjorstad, and Gropp (1996)]. We should make a note here that it is growing popular, due to many common features, to collectively refer MG and DD methods as Schwarz methods. However, we should also mark that the mere fact of basis functions being hierarchical is not sufficient to result in efficient matrix solution. Particularly, for matrix equations resulting from the discretization of Maxwell equations, the two approaches outline by Webb [Webb] and Sun-Lee-Cendes [Sun, Lee, and Cendes (2001)] are promising not only because they are hierarchical but also because they are split into two groups – pure gradient basis functions and their complements, a discrete version of the Helmholtz decomposition. We shall report it in a later contribution that with explicitly forming the gradient basis functions and a trivial diagonal scaling, the notorious null space of the curl operator will be converted from negative eigenmodes into positive eigenmodes in deterministic frequency domain applications. Subsequently, for TVFEMs that mimic in-exact Helmholtz decomposition, the only negative eigenmodes are the physical modes that are resonant below the operating frequency. Although, theoretically these negative modes can still render the resulting matrix equations highly indefinite for electrically-large problems, fortunately, in many practical applications, such problem can be circumvented satisfactorily using MG or Schwarz method provided the mesh is sufficient fine to model these negative modes. Furthermore, we comment that the approach outlined by Webb [Webb] does indeed explicitly forming the gradient basis functions for the higher order spaces; however, in the lowest order space, the conventional edge elements were employed. To achieve the near-optimal performance of the Schwarz method (the number of iterations remain almost unchanged when matrix dimensions increase), we strongly advocate the splitting of edge elements by means of tree-cotree partition of the finite element mesh [Albanese and Rubinacci (1998)]. A similar rationale can be found in integral equation too, and it was mainly referred to as loop-star and/or loop-tree basis functions [Lee, Burkholder, and Lee (2003)].

As mentioned earlier, in recent years, researchers have found that the popular MG methods and DD methods share many common features, and the main ingredients can be traced back to the paper published by Schwarz at 1870 [Schwarz (1870)]. Subsequently, it is becoming accepted to collectively refer them as Schwarz methods. The particular Schwarz method that we adopted herein is a multiplicative scheme and we treat each polynomial space as a domain. We shall refer to this particular approach p-type multiplicative Schwarz method (pMUS). The technical details of pMUS will be discussed in later section. However, we like to point out that since there are still negative eigenmodes exist in the formulation (resonant modes below the operating frequency), the success of Schwarz methods in turn depends on whether the "coarse" grid, in this case the co-tree edge elements space, can accurately model these negative modes. Thus, for a given physical problem, there exists a minimum mesh (or maximum discretization size) such that Schwarz methods can converge. It is found that the multiplicative Schwarz method is not only more robust (it converges when the additive version fails) but also requires less number of iterations compare to the additive version [Smith, Bjorstad, and Gropp (1996)][Peng, Dyczij-Edlinger, and Lee (1999)].

The approach used to solve the electromagnetic problem in this paper is based on a frequency domain solver. An alternate approach is to solve the problem in the time domain [Hassan, Morgan, Jones, Larwood, and Weatherill (2004)], [Hesthaven and Warburton (2004)]. Time domain approaches allow one to obtain a solution over a wide bandwidth with a single run. However, frequency domain methods can also be used to obtain wide-band solution in an efficient manner through the use of reduced order models [Reddy (2004)].

The rest of this paper is organized as follow. Section II discussed the hierarchical basis functions (p = 2) that we employed in this study, the technical details of the pMUS are included in Section III, a few numerical examples (waveguide discontinuities) are shown in Section IV along with the needed computer resources to model them, finally we conclude and make a few futuristic remarks in Section V.

2 Basis functions used in the FEM frequency domain codes

2.1 Time Harmonic Maxwell's Equations

The boundary value problem (B.V.P.) can be described in a general way as a multiport microwave device as: (em-

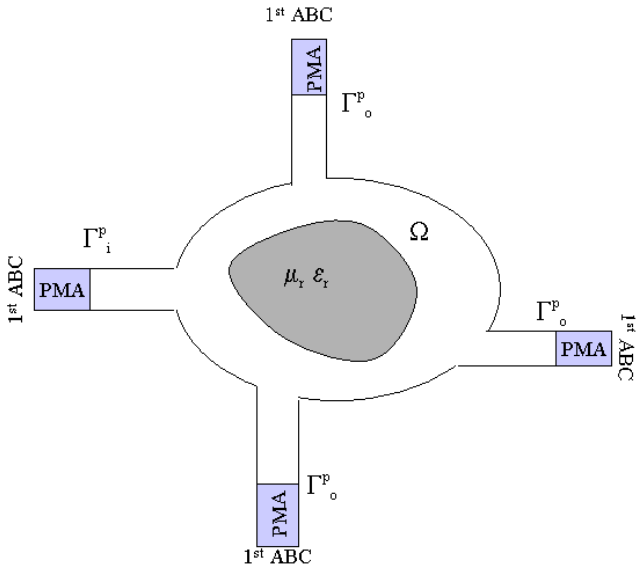

Figure 1 : A multiport waveguide discontinuity/junction with PMA automatically patched to back up all the ports to absorb waves.

ploying field formulation)

$$\nabla \times \frac{1}{\mu_r} \nabla \times \vec{E} - k^2 \varepsilon_r \vec{E} = 0 \text{ in } \Omega$$
$$\left[\hat{n} \times \nabla \times \vec{E}\right]_{\Gamma_i^p} = -j\omega\mu_0 \vec{J}_i^p$$
$$\hat{n} \times \vec{E}\,|_{\Gamma_{pec}} = 0$$
$$\hat{n} \times \nabla \times \vec{E}\,|_{\Gamma_{pmc}} = 0$$
$$\hat{n} \times \nabla \times \vec{E}\,|_{\Gamma_\infty} = -jk\frac{\eta}{Z}\left(\hat{n} \times \hat{n} \times \vec{E}\right)|_{\Gamma_\infty} \quad (1)$$

A description of notations is in order here. The notation $\vec{v}|_\Gamma$ denotes the restriction of vector field $\vec{v}$ to Γ, $[\hat{n} \times \vec{v}]_\Gamma$ means the jump of $\hat{n} \times \vec{v}$ across boundary Γ. Also note in Eq. (1), we have used Γ_i^p to indicate the input port where a specified surface current density, $\vec{J}_i^p$, exists. In Figure 1, we have also employed symbol Γ_o^p to denote output port planes. Furthermore, once a plane is identified as a port plane, three layers of perfectly matched absorber (PMA) will automatically be added behind the port plane to absorb wave propagates out from the problem domain. To make the PMAs even more effectively, we back up the PMA with an 1^{st} order ABC at the very end of the PMAs. The theory and properties of PMA are very well documented in many articles; we are not going to elaborate much here about our choice of PMAs except to say they are constructed in an implicit manner such that no physical mesh is ever created. Note also that in Eq. (1), we use Γ_{pec} and Γ_{pmc} for perfect electric and magnetic conductors, respectively. The notation Γ_∞ is adopted to denote the boundary where radiation boundary condition needs to be imposed. We plan to implement integral equation for mesh truncation in the future, however, currently the mesh truncation method, or the radiation condition is the 1^{st} order absorbing boundary condition (ABC) with user specified impedance, Z.

2.2 Bilinear Form and p=2 Vector Basis Functions

Corresponds to Eq. (1), the finite dimensional weak statement of the formulation can be stated as:

Seek $\vec{u}^h \in V^h \subset H_0(curl)$ such that
$$B\left(\vec{v}^h, \vec{u}^h\right) = F\left(\vec{v}^h\right) \ \forall \vec{v}^h \in V^h$$
where $B\left(\vec{v}^h, \vec{u}^h\right)$
$$= a\left(\vec{v}^h, \vec{u}^h\right) - k^2\left(\vec{v}^h, \vec{u}^h\right)_{\Omega^h} - jk\frac{\eta}{Z}\left\langle \vec{v}^h, \vec{u}^h \right\rangle_{\Gamma_\infty}$$
and $F\left(\vec{v}^h\right) = jk\eta\left\langle \vec{v}^h, \vec{J}_i^p \right\rangle_{\Gamma_i^p}$ (2)

In Eq. (2), a few notations are defined by

$$a\left(\vec{v}^h, \vec{u}^h\right) = \int_{\Omega^h} \nabla \times \vec{v}^h \circ \frac{1}{\mu_r} \nabla \times \vec{u}^h d\Omega;\ \left(\vec{v}^h, \vec{u}^h\right)_{\Omega^h}$$
$$= \int_{\Omega^h} \vec{v}^h \circ \varepsilon_r \vec{u}^h d\Omega;\ \left\langle \vec{v}^h, \vec{u}^h \right\rangle_\Gamma$$
$$= \int_\Gamma \vec{v}^h \circ \left(\hat{n} \times \hat{n} \times \vec{u}^h\right) d\Gamma \quad (3)$$

The discretization, or the finite element process, that we have adopted here is the first-kind Nedelec curl conforming basis functions (p = 2) on tetrahedral mesh. Specifically, given a tetrahedral mesh Ω^h, our finite dimensional test/trial space can be written as a direct sum as

$$V^h = \nabla\varsigma_i^h \oplus \vec{W}_{cT}^h \oplus \nabla\left(\varsigma_i^h \varsigma_j^h\right) \oplus R_2^f \quad (4)$$

Consequently, in a tetrahedron, there would be at most

24 degrees of freedom. They are:

p = 1

vertex i : $\nabla\varsigma_i$

co - tree edge $\{i,j\}$: $\varsigma_i\nabla\varsigma_j - \varsigma_j\nabla\varsigma_i$

p = 2

edge $\{i,j\}$: $\nabla(\varsigma_i\varsigma_j)$

face $\{i,j,k\}$: $\begin{cases} \varsigma_i(\varsigma_j\nabla\varsigma_k - \varsigma_k\nabla\varsigma_j) \\ \varsigma_j(\varsigma_k\nabla\varsigma_i - \varsigma_i\nabla\varsigma_k) \end{cases}$ (5)

Note that in the lowest level, the inexact-Helmholtz splitting is accomplished by a tree-cotree splitting. Namely, we will keep the edge elements basis functions on co-tree edges. Subsequently, for a discretization Ω^h, the number of unknowns is

$$N = V + (E - V) + E + 2F = 2E + 2F \tag{6}$$

where V, E, F are the number of vertexes, edges, and triangular faces, respectively.

3 Schwarz matrix solution techniques

3.1 pMUS as a p-Schwarz Domain Decomposition Method

In our work, we employ Schwarz methods, often used in the domain decomposition area, and apply them to form an efficient preconditioner for the conjugate gradient algorithm with p-type finite elements (in current case, p = 2). Schwarz introduced the earliest domain decomposition method in 1870. Though not originally intended as a numerical method, the classical alternating Schwarz method has been used intensively to solve elliptic boundary value problems on domains that are the union of two subdomains by alternatingly solving the same elliptic boundary problem restricted to the individual subdomains. However, our work focus on the use of p-type finite elements, and treating each p group as a *domain*, subsequently, in our current interpretation, our domains do not overlap. Thus, the Schwarz method that we employed here in a non-overlapping Schwarz method, or more specifically the Schur complement method. In particular, we use a multiplicative Schwarz preconditioner. This structure, as mentioned, can be viewed as a non-overlapping block Gauss-Seidel preconditioner. Even without the conjugate gradient acceleration, the multiplicative method can take far less iteration than the additive version. This theory is provided in [Bramble, Pasciak, Wang, and Xu (1991)]. Conventionally, multilevel methods are associated with a nested grid that employs a multilevel of grids [Hiptmair (1998)]. In this work, the multilevel algorithm employs a single grid but a multilevel of basis functions. We may think of the approach presented here as a p-refinement multilevel method [Sun, Lee, and Cendes (2001)] instead of the more traditional h-refinement multilevel method, where p refers to the order of the element and h refers to the element size. We employ the Schur factorization to obtain an approximate inverse of the system matrix and treat it as a preconditioner in the conjugate gradient method. It can be proved that the current approach is equivalent to a V-cycle multigrid method. An advantage of the current approach is that it provides a better understanding of the approximation made in computing the preconditioner. We will call the resulting procedure the pMUS method.

3.2 P-type Multiplicative Schwarz Method (pMUS)

Numbering the unknowns from p = 1 group (the vertex gradients and the co-tree edge elements) to the p = 2 group, the system matrix $\mathbf{A}$ is partitioned into a 2 by 2 block matrix as

$$\mathbf{A} = \begin{bmatrix} \mathbf{A_{1,1}} & \mathbf{A_{1,2}} \\ \mathbf{A_{2,1}} & \mathbf{A_{2,2}} \end{bmatrix} \tag{7}$$

A word of caution here: since the vector basis functions are of very different natures, their diagonal entries in the system matrix will vary drastically, therefore, it is always a good practice to diagonal scaling the system matrix first before apply matrix solution techniques. Consequently, the system matrix $\mathbf{A}$ in (7) refers the matrix after the scaling, thus, all its diagonal entries are 1.0. The Schur factorization process begins by recognizing that the matrix $\mathbf{A}$ can be written in a product form as

$$\begin{aligned} \mathbf{A} &= \begin{bmatrix} \mathbf{A_{1,1}} & \mathbf{A_{1,2}} \\ \mathbf{A_{2,1}} & \mathbf{A_{2,2}} \end{bmatrix} \\ &= \begin{bmatrix} \mathbf{I} & \mathbf{0} \\ \mathbf{A_{2,1}A_{1,1}^{-1}} & \mathbf{I} \end{bmatrix} \begin{bmatrix} \mathbf{A_{1,1}} & \mathbf{0} \\ \mathbf{0} & \mathbf{A_{2,2} - A_{2,1}A_{1,1}^{-1}A_{1,2}} \end{bmatrix} \\ &\quad \begin{bmatrix} \mathbf{I} & \mathbf{A_{1,1}^{-1}A_{1,2}} \\ \mathbf{0} & \mathbf{I} \end{bmatrix} \end{aligned} \tag{8}$$

Subsequently, we perform two incomplete Choleski factorization with different threshold values for sub-

matrices $\mathbf{A_{1,1}}(1.0e^{-5})$ and $\mathbf{A_{2,2}}(1.0e^{-2})$. Namely

$$\begin{array}{ll} \mathbf{A_{1,1}} = \mathbf{C_{1,1}^t C_{1,1}} + \mathbf{E_1} & \|\mathbf{E_1}\| \leq 1.0e^{-5} \\ \mathbf{A_{2,2}} = \mathbf{C_{2,2}^t C_{2,2}} + \mathbf{E_2} & \|\mathbf{E_2}\| \leq 1.0e^{-2} \end{array} \tag{9}$$

Equation (9) simply states that we drop entries in the factorization process that are smaller than $1.0e^{-5}$ and $1.0e^{-2}$ for $\mathbf{A_{1,1}}$ and $\mathbf{A_{2,2}}$, respectively. With $\mathbf{C_{1,1}}$ and $\mathbf{C_{2,2}}$obtained, our preconditioner takes the form

$$\begin{aligned} \mathbf{M} = & \begin{bmatrix} \mathbf{I} & \mathbf{0} \\ \mathbf{A_{2,1}} \left(\mathbf{C_{1,1}^t C_{1,1}}\right)^{-1} & \mathbf{I} \end{bmatrix} \\ & \begin{bmatrix} \left(\mathbf{C_{1,1}^t C_{1,1}}\right) & \mathbf{0} \\ \mathbf{0} & \left(\mathbf{C_{2,2}^t C_{2,2}}\right) \end{bmatrix} \\ & \begin{bmatrix} \mathbf{I} & \left(\mathbf{C_{1,1}^t C_{1,1}}\right)^{-1} \mathbf{A_{1,2}} \\ \mathbf{0} & \mathbf{I} \end{bmatrix} \end{aligned} \tag{10}$$

Once the preconditioner $\mathbf{M}$ is written in the product form in Eq. (10), its inverse is readily available by

$$\begin{aligned} \mathbf{M}^{-1} = & \begin{bmatrix} \mathbf{I} & -\left(\mathbf{C_{1,1}^t C_{1,1}}\right)^{-1} \mathbf{A_{1,2}} \\ \mathbf{0} & \mathbf{I} \end{bmatrix} \\ & \begin{bmatrix} \left(\mathbf{C_{1,1}^t C_{1,1}}\right)^{-1} & \mathbf{0} \\ \mathbf{0} & \left(\mathbf{C_{2,2}^t C_{2,2}}\right)^{-1} \end{bmatrix} \\ & \begin{bmatrix} \mathbf{I} & \mathbf{0} \\ -\mathbf{A_{2,1}} \left(\mathbf{C_{1,1}^t C_{1,1}}\right)^{-1} & \mathbf{I} \end{bmatrix} \end{aligned} \tag{11}$$

Using Eq. (11) as the preconditioner in the preconditioned conjugate gradient method results in the pMUS method that is adopted in the current work. Its performance for solving matrix equations arisen from the vector finite elements (p = 2) for Maxwell's equation is truly remarkable. We would also like to make additional comment about the splitting of the edge elements using the tree-cotree approach. It is possible just to employ the edge elements in its entirety and still apply the pMUS method to solve the resulting matrix equations. The convergence is in general equally as good as in the current approach. However, there are two major advantages to advocate the splitting: 1. The splitting allows us to employ incomplete Choleski factorization instead of complete factorization that is in general needed for pure edge elements; and, 2. By using the pure edge elements for p = 1 block, we observed the failure to converge when very small elements are present in the problem domain, whereas in the current approach, the problem simply goes away. This is mainly due to the low frequency instability and Gaussian elimination without extensive pivoting will suffer greatly round-off errors for poor conditioned matrices.

4 Numerical results

4.1 A seven-section waveguide transformer

This example is a waveguide transformer which connects an input waveguide, with dimensions 16.51 x 8.255 $(cm)^2$, to a smaller waveguide, with dimensions 16.51 x 1.016 $(cm)^2$, through seven waveguide sections. The wide side of the waveguides are kept the same, namely a = 16.61 cm. The dimensions of the narrow side of the seven sections as well as their lengths are summarized in Table 1.

	b (cm)	L(cm)
1	7.87494	7.18744
2	6.65247	7.03537
3	4.74347	6.89166
4	2.97030	6.89697
5	1.84134	6.98825
6	1.28891	7.05869
7	1.07201	7.12572

Table 1 : Dimensions of the narrow side of the seven waveguide sections for the seven-section waveguide transformer.

The problem has 2 symmetries making it possible to be simulated using only $1/4$ of the geometry, as seen in Figure 2.

We adaptively refine the mesh at 1GHz, 1.3 GHz, 1.6 GHz, and 1.8 GHz, with the error tolerance set to be 0.2%. The process results in a mesh as shown in Figure . This mesh corresponds to 30,150 unknowns using p = 2 first-kind Nedelec vector basis functions. Figure 3 shows the color plot of the field distribution of the waveguide transformer at 1.45 GHz. The comparison of the VSWR computed by using the current finite element frequency domain approach with those obtained by Bakr et. al is

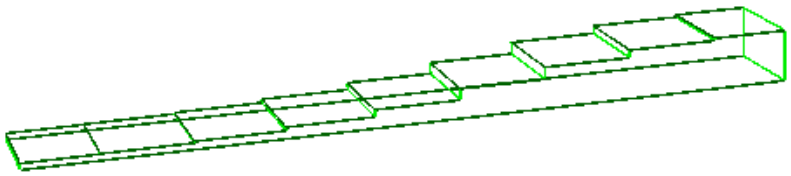

Figure 2 : A 1/4 of the geometry is input into the computer for simulation. The bottom of the model, a symmetric plane, is assigned PEC whereas one side wall, another symmtric plane, is assigned PMC.

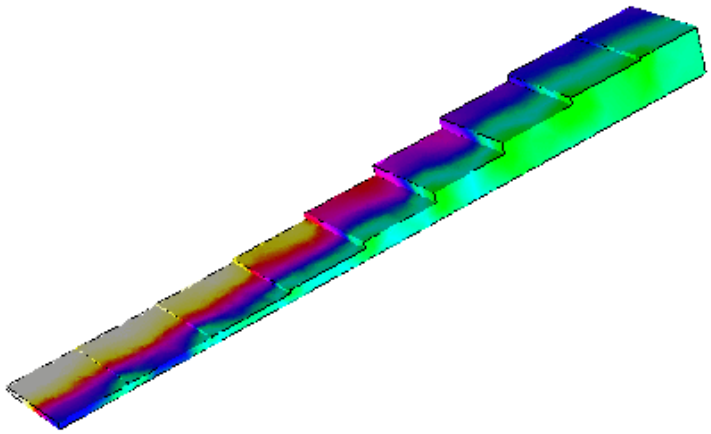

Figure 3 : Field distribution of the seven-section waveguide transformer at 1.45GHz.

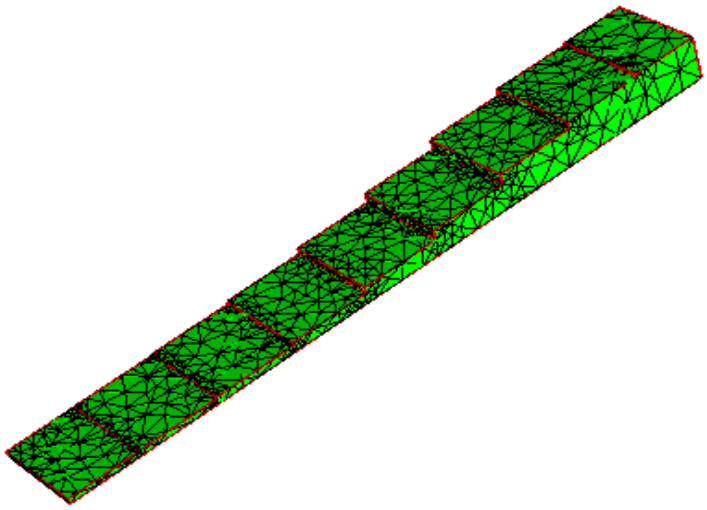

Figure 4 : The final mesh for the seven-section waveguide transformer. It is adaptively refined at 1, 1.3, 1.6, and 1.8 GHz with error tolerance 0.2%.

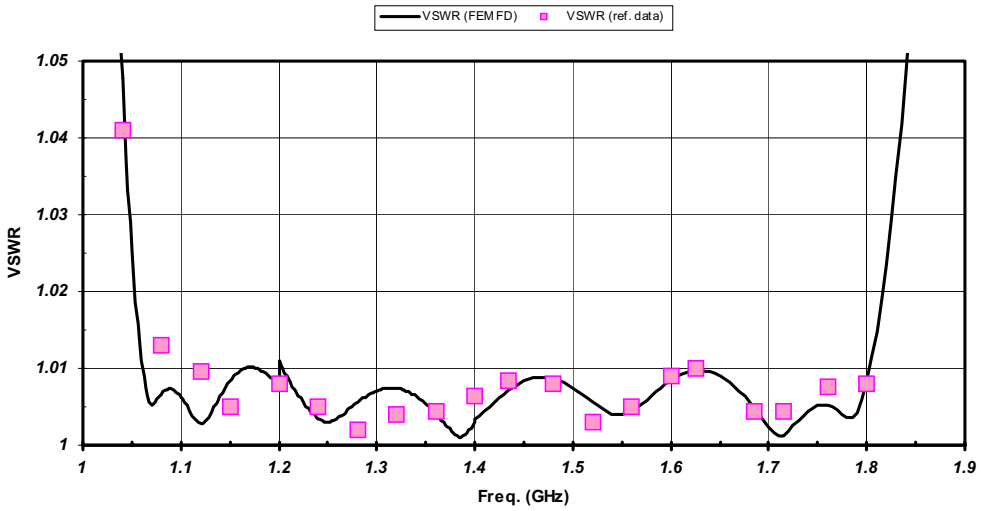

Figure 5 : The computed VSWR compared to reference data obtained by Bakr et. al using Ansoft Maxwell Eminence[4].

plotted in Figure 5[4].

4.2 A five-cavity e-plane waveguide band-pass filter

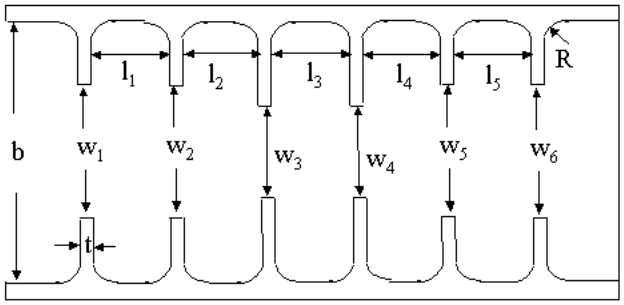

Figure 6 : A five-cavity E-plane waveguide band-pass filter.

Shown in Figure 6 is a five-cavity E-plane waveguide band-pass filter. This structure was first analyzed by Reiter and Arndt [Arndt and Reiter (1995)]. The width of the entire filter is 47.55 mm, and the rest of the dimensions in Figure 6 are summarized in Table 2.

We adaptively refine the mesh for the waveguide band-pass filter at 3.43, 4.0, and 4.3 GHz with error tolerance δ=0.03, the final mesh is shown in Figure 8. Note that,

[4] Maxwell Eminence is a trademark of Ansoft Corp., Pittsburgh, PA 15219, USA.

b=22.149	l_1=l_5=21.817	w_1=w_6=9.99
t=3	l_2=l_4=14.726	w_2=w_5=3.497
R=5	l_3=11.999	w_3=w_4=1.693

Table 2 : Dimensions, in mm, for the five-cavity E-plane waveguide band-pass filter.

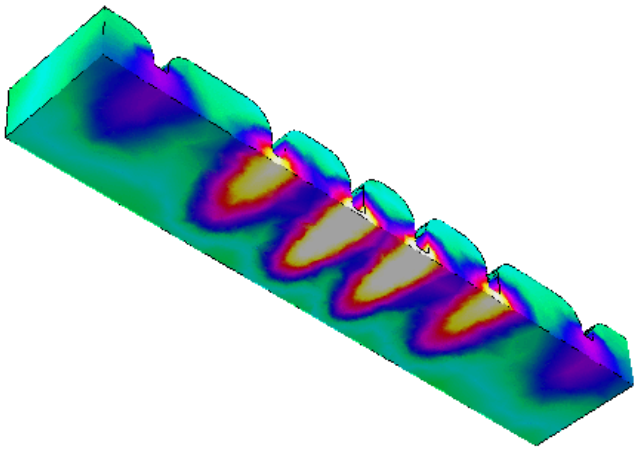

Figure 7 : Electric field distribution for the waveguide band-pass filter at 4.0 GHz.

once again, due to 2-way symmetry, only 1/4 of the geometry has been included in the computer model. The electric field distribution for the filter at 4 GHz is plotted in Figure 7. The mesh shown in Figure 8, corresponds

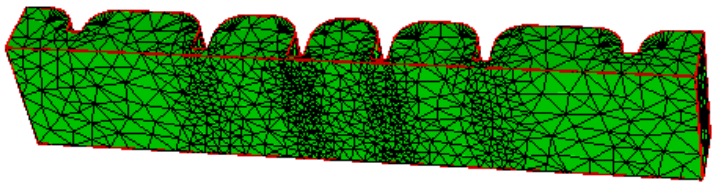

Figure 8 : The final mesh of the five-cavity E-plane waveguide band-pass filter. Adaptively refined at 3.43, 4.0, and 4.3 GHz with δ= 0.03.

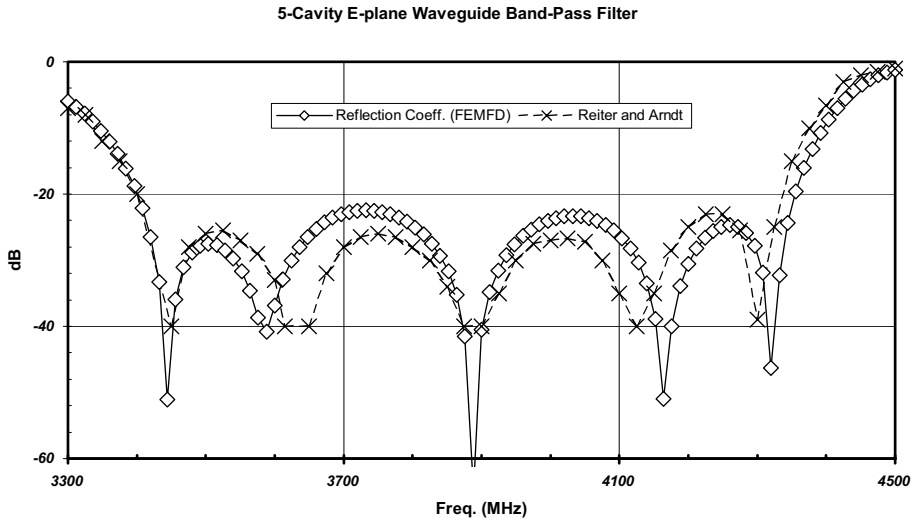

Figure 9 : The computed reflection coefficients, from 3.3 to 4.5 GHz, compared to those obtained previously using a generalized mode matching technique by Reiter and Arndt.

to 108,842 (p=2, first-type Nedelec curl conforming elements), is then used to generate the entire spectral response from 3.3 to 4.5 GHz. We compare the computed results, reflection coefficient, to those obtained by Reiter and Arndt [Arndt and Reiter (1995)] using a generalized mode-matching technique. Within the spectral, as can be seen from the figure, there is noticeable discrepancy between the current FEM approach and the Reiter-and-Arndt results. It is our belief that the current FEM approach provides much more accurate numerical solutions than the generalized mode-matching method. In particular, the fact that the five cavity chambers in the filter are all with rounded corners, which is known to be difficult to account for in mode-matching like techniques.

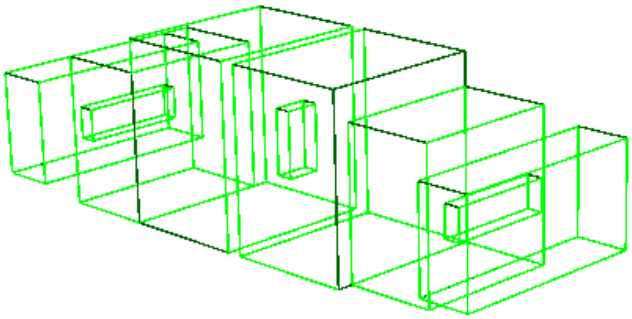

Figure 10 : Wireframe of a rectangular waveguide dual-mode filter.

4.3 A Rectangular waveguide dual-mode filter

Shown in Figure 10 is a wireframe plot of a rectangular waveguide dual-mode filter. This example is taken directly from Ref. [Bornemann, Rosenberg, Amari, and Vahldieck (1999)], and its exact dimensions of each cross-section are also listed therein. In the current approach, we first adaptively refine the mesh, using an h-version adaptive mesh refinement process, at 12.3 GHz with a target error of 1%. The h-adaptive mesh refine-

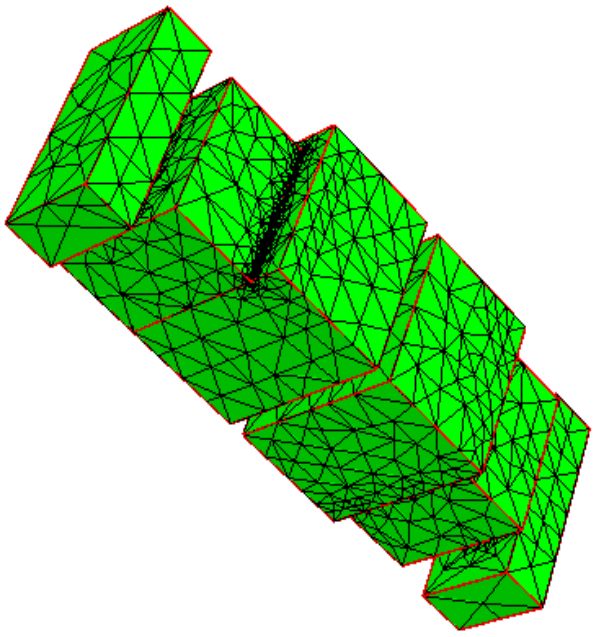

Figure 11 : Tetrahedral mesh generated through adaptive mesh refinement at 12.3 GHz with 1% target error for the rectangular waveguide dual-mode filter.

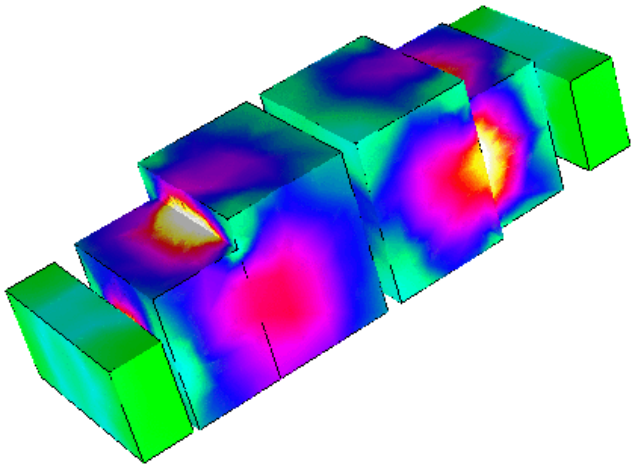

Figure 12 : Field plot for the rectangular waveguide dual-mode filter at 12.3 GHz.

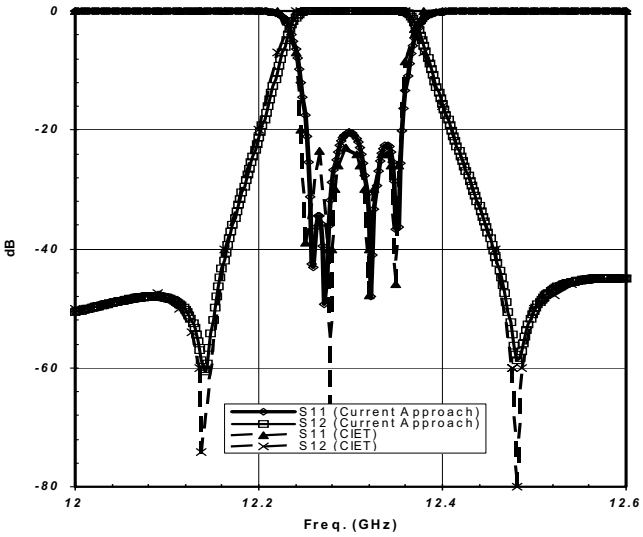

Figure 13 : Responses, S11 and S12, for the rectangular waveguide dual-mode filter.

ment results in a non-uniform mesh as shown in Figure 11. We also include the field plot at the 12.3 GHz in Figure 12. This mesh corresponds to 232,454 unknowns using first-kind p=2 Nedelec curl-conforming vector finite elements. Using the 2-level Schwarz method, it took 18 iterations to solve the matrix equation with a relative residual smaller than 10^{-4}. Also, the memory required was only 170 MB. This compares very favorably with the HFSS results obtained by Bornemann et. al. in Ref. [Bornemann, Rosenberg, Amari, and Vahldieck (1999)], which was reported exceeded 500 MB. Figure 13 plots the responses obtained using the current approach against those taken from Ref. [Bornemann, Rosenberg, Amari, and Vahldieck (1999)]. The agreement between the FEM data and the CIET results is very good as can be seen from the figure.

4.4 A 4-Iris TE_{01} Circular waveguide bandpass filter

This example is a bandpass filter made of a TE_{01} mode circular waveguide with 4 iris inserted. The dimensions of the waveguide as well as the irises and their separations are indicated in the cross-sectional plot in Figure 14. This example was first studied by Papziner and

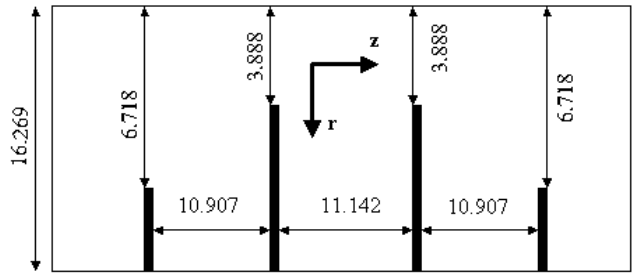

Figure 14 : The dimensions, cross-sectional view, of a 4-iris TE01 circular waveguide bandpass filter.

Arndt [Papziner and Arndt (1993)], and later by Amari, Bornemann, Laisne, and Vahldieck [Amari, Bornemann, Laisne, and Vahldieck (2001)]. Note that there was a minor mistake in reference [Amari, Bornemann, Laisne, and Vahldieck (2001)] about the inner radii of the irises. Since the bandpass filter was excited by a TE_{01} mode from the empty circular waveguide, we only modeled 1/8 of the iris-coupled waveguide as suggested in Ref. [Amari, Bornemann, Laisne, and Vahldieck (2001)]. The wireframe model of the iris-coupled circular waveguide employed in our analysis is shown in Figure 15. The structure was first undergone an h-version adaptive mesh refinement in the FEM process at 11.741 GHz with a target error of 1%. It resulted in a final mesh shown in Figure 16. The corresponding field plot at 11.741 GHz is also included in Figure 17. Subsequently, the same mesh, as shown in Figure 16, is employed in a fast frequency sweep algorithm using AWE-like technique to obtain the spectral responses of the return loss. The return loss of the iris-coupled waveguide, from 17.45 GHz to 17.54 GHz, as well as its comparisons to the CIET and HFSS[5] results reported in Ref. [Amari, Bornemann, Laisne, and Vahldieck (2001)] are plotted in Figure 18. Note that our current approach yields a better agreement with CIET technique than the HFSS results taken from Ref. [Amari, Bornemann, Laisne, and Vahldieck (2001)]. Even more strikingly is the fact according to Ref. [Amari, Bornemann, Laisne, and Vahldieck (2001)], the HFSS results were obtained using resources exceeded 800 MB. In the current approach, the results were computed using p=2 first-kind Nedelec curl-conforming elements with 338,032 unknowns and it took only 254 MB to complete the simulation. Therefore, it is demonstrated in this example that using the proposed Schwarz method to solve the matrix equations from hierarchical vector finite element methods results in significant reduction in terms of computer resources. Hence, more accurate and less resources-taxing numerical simulations can be performed than the commercial software that is available today.

4.5 Performances of the Schwarz method

In Table 3, we summarize the performances of the proposed Schwarz method to solve the matrix equations for the numerical examples studied in this paper. In Table 3, N stands for the number of unknowns (corresponds to p=2 first-kind Nedelec curl conforming elements), NZ is the total nonzero entries in the matrix, NZ (PC) is the number of nonzero entries in the preconditioning matrix, CPU (PC) is the CPU time needed to construct the preconditioning matrix, CPU (CG) denotes the CPU time for solving the matrix equation using the Conjugate Gradient method with a relative residual of 10^{-4}, in the Memory column, the maximum amount of memory needed for the examples are listed, and the N_{CG} lists the number of iterations in the CG process to reduce the relative residual to 10^{-4}. It is noted from Table 3, and is generally true for all applications that we run, the sizes of the preconditioning matrices (NZ (PC)) are always smaller than the origi-

[5] HFSS is a product of Ansoft Corp. Pittsburgh, PA 15213.

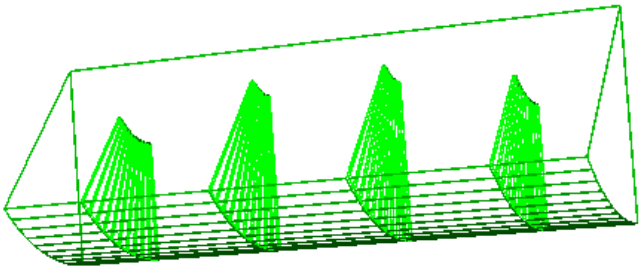

Figure 15 : The wireframe of the geometry used for the computer simulation using the FEM frequency domain approach.

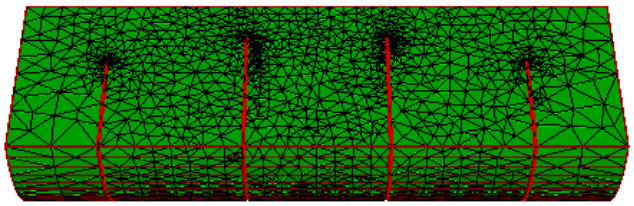

Figure 16 : The final tetrahedral mesh after h-adaptive mesh refinement at 17.491 GHz and with a tolerance of 1%.

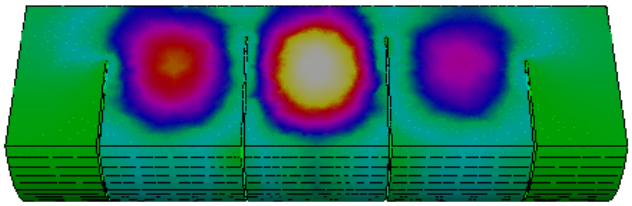

Figure 17 : Field plot at 17.49 GHz.

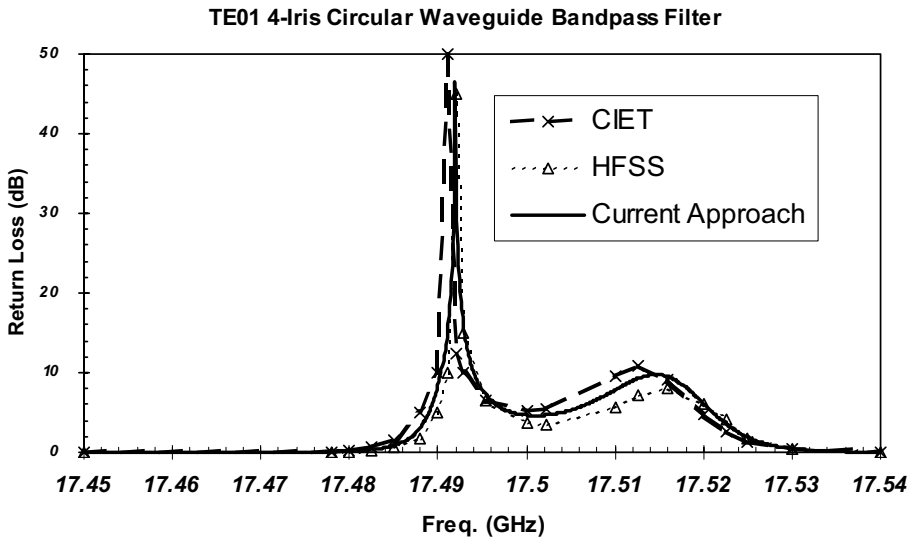

Figure 18 : The return loss of the circular waveguide bandpass filter using the current FEM approach compared to results obtained by CIET and using HFSS.

N	NZ	NZ (PC)	CPU (PC)	CPU (CG)	N_{CG}	Memory
30,356 (WGX)	633,341	302,479	$<$ 1 s	6 s	16	16 MB
108,842 (EPF)	2,391,207	1,347,553	8 s	35 s	21	67 MB
232,454 (DMF)	5,500,914	3,626,860	68 s	73 s	18	170 MB
338,032(CWG)	8,038,555	5,739,966	150 s	154 s	24	254 MB

Table 3 : Performance of the proposed 2-level Schwarz method applied to hierarchical vector finite elements with tree-cotree splitting.

nal matrix equations (NZ). Note also, in Table 3, (WGX) is the for the waveguide transformer example, (EPE) for E-plane waveguide filter, (DMF) is for the rectangular waveguide dual-mode filter, and (CWG) denotes for the circular waveguide 4-iris bandpass filter.

5 Conclusions

We proposed in this paper an approach to solve three-dimensional Maxwell's equations in the frequency domain. The curl-conforming basis functions inspired by Nedelec [Nedelec (1980)] are constructed in a hierarchical way. Furthermore, it is strongly advocate the basis functions need further be divided into two groups: pure gradient basis functions and their compliments. This is in-line with the continuous Helmholtz decomposition, and in a more general setting consistent with the de-Rham diagram suggested in [Hiptmair (1999)]. Note also that in the lowest order, the edge elements, the splitting is accomplished through a graph partition, namely the tree-cotree splitting. Hierarchical basis functions constructed this way would not suffer the troublesome low-frequency instability which hinder the success of h-version adaptive mesh refinement for general applications. More importantly, current way of constructing basis functions lend itself naturally into a p-type multiplicative Schwarz method (pMUS) which only requires in-complete LU decomposition of the diagonal block in the system matrices to form a very effective preconditioner. The performance of the pMUS approach proposed in this paper for solving waveguide discontinuities is truly remarkable. It compares very favorably with current existing commercial software both in terms of memory as well as CPU times.

References

Albanese, R.; Rubinacci, G. (1998): Solution of three dimensional eddy current problems by integral and differential methods, *IEEE Trans. Magn.* vol. MAG-24, pp. 98-101.

Amari, S.; Bornemann, J.; Laisne, A.; Vahldieck, R. (2001): Design and Analysis of Iris-Coupled and Dielectric-Loaded 1/8 Cut TE_{01}-mode Microwave Bandpass Filters, *IEEE Trans. Microwave Theory and Techniques*, vol. 49, no. 3, pp. 413-421.

Arndt, F.; Reiter, J. M. (1995): Rigorous Analysis of Arbitrarily Shaped H- and E-Plane Discontinuities in Rectangular Waveguides by a Full-Wave Boundary Contour Mode-Matching Method, *IEEE Trans. Microwave Theory Tech.*, 43:pp. 796-801.

Bornemann, J.; Rosenberg, U.; Amari, S.; Vahldieck, R. (1999): Edge-Conditioned Vector Basis Functions for the Analysis and Optimization of Rectangular Waveguide Dual-Mode Filters, IEEE MTT-S Int. Microwave Symp. Dig. Anaheim, CA, pp. 1695-1698.

Bramble, J. H.; Pasciak, J. E.; Wang, J.; Xu, J. (1991): Convergence estimates for product iterative methods with applications to domain decompositions and multigrid, *Math. Comp.*, 57, pp. 1-21.

Duff, S.; Reid, J. K. (1983): The Multifrontal Solution of Indefinite Sparse Symmetric Linear Equations, *ACM Trans. Math. Softw.*, vol. 9, pp. 302-325.

Hassan, O.; Morgan, K.; Jones, J.; Larwood, B.; Weatherill, N. P. (2004): Parallel 3D Time Domain Electromagnetic Scattering Simulations on Unstructured Meshes, *CMES: Computer Modeling in Engineering & Sciences*, vol. 5, no. 5, pp. 383-394.

Hesthaven, J. S.; Warburton, T. (2004): High-Order Accurate Methods for Time-domain Electromagnetics, *CMES: Computer Modeling in Engineering & Sciences* , vol. 5, no. 5, pp. 395-408.

Hiptmair, R. (1998): Multigrid method for Maxwell's equations, *SIAM J. Numer. Anal.*, 36, pp. 204-225.

Hiptmair, R. (1999): Canonical Construction of Finite Elements, *Math. Comp.*, vol. 68, pp. 1325-1346.

Karypis, G.; Kumar, V. (1998): METIS 4.0: Unstructured graph partitioning and sparse matrix ordering system. Technical report, Dept. of Computer Science, University of Minnesota. Available on the WWW at URL http://www.cs.umn.edu/∼metis.

Lee, J.-F. (1990): Analysis of Passive Microwave Devices by Using Three-Dimensional Vector Finite Elements, *Int. J. Num. Modeling*, 3:235-246.

Lee, J.-F.; Burkholder, R.; Lee, R. (2003): Loop Star Basis Functions and a Robust Preconditioner for EFIE Scattering Problems, *IEEE Trans. Antenna Propag.*, AP-51, pp. 1855-1863.

Lee, J.-F.; Sun, D.-K.; Cendes, Z. J. (1991): Tangential Vector Finite Elements for Electromagnetic Field Computation, *IEEE Trans. Magn.*, vol. 27, pp. 4032-4035.

Li, M.; Zhang, Q.-J.; Nakhla, M. (1996): Finite Difference Solution of EM Fields by Asymptotic Waveform Techniques, *IEE Proc. H, Microw. Antennas Propag.*, vol. 143, no. 6, pp. 512-520.

Nedelec, J. C. (1980): Mixed Finite Elements in R3, Numer. Math., vol. 35, pp. 315-341.

Papziner, U.; Arndt, F. (1993): Field Theoretical Computer-Aided Design of Rectangular and Circular Iris Coupled Rectangular or Circular Waveguide Cavity Filters, *IEEE Trans. Microwave Theory and Techniques*, vol. 41, no. 3, pp. 462-471.

Peng, G.; Dyczij-Edlinger, R.; Lee, J.-F. (1999): Hierarchical Methods for Solving Matrix Equations from TVFEMs for Microwave Components, *IEEE Trans. Magn.*, vol. 35, pp. 1474-1477.

Reddy, C. J. (2004): Application of MBPE Method to Frequency Domain Hybrid Techniques to Compute RCS of Electrically Large Objects, *CMES: Computer Modeling in Engineering & Sciences*, vol. 5, no. 5, pp. 455-462.

Schwarz, H. A. (1870): Gesammelte Mathematische Abhandlungen, vol. 2, pp. 133-143, Springer Berlin, 1890. First published in Vierteljahrsschrift Naturforsch. Ges. Zurich, 15: 272-286.

Smith, B.; Bjorstad, P.; Gropp, W. (1996): Domain Decomposition – Parallel Multilevel Methods for Elliptic Partial Differential Equations, Cambridge University Press.

Sun, D.-K.; Lee, J.-F.; Cendes, Z. J. (2001): Construction of Nearly Orthogonal Nedelec Bases for Rapid Convergence with Multilevel Preconditioned Solvers, *SIAM J. Sci. Comput.*, vol. 23, pp. 1053-1076.

Webb, J. P. : Hierarchical Vector Basis Functions of Arbitrary Order for Triangular and Tetrahedral Finite Elements, *IEEE Trans. Antennas Propagat.*, vol. 47, pp. 1244-1253.

Webb, J. P.; Forghani, B. (1993): Hierarchical Scalar and Vector Tetrahedra, *IEEE Trans. Magn.*, vol. 29, pp. 1495-1498.